https://doi.org/10.5194/essd-2025-674
Preprint. Discussion started: 8 January 2026

Open Access Earth System Science Data Discussions

A global map of forest age for natural and planted forests at a fine spatial resolution of 30 meters

Authors

Yan Wang[1], Hengbin Wang[1], Chaoran Liang[1], Xiyi Li[1], Zhe Liu[1,2,3], Xiaodong Zhang [1,2,3], Shaoming Li[1,2,3], Yuanyuan Zhao[1,2,3*]

1 College of Land Science and Technology, China Agricultural University, Beijing 100083, China; wangyan@cau.edu.cn; hbwang@cau.edu.cn; s20253213945@cau.edu.cn; lixiyi@cau.edu.cn; liuz@cau.edu.cn; zhangxd@cau.edu.cn; lshaoming@sina.com; zhaoyuanyuan@cau.edu.cn.

2 Key Laboratory of Remote Sensing for Agri-Hazards, Ministry of Agriculture and Rural Affairs, Beijing 100083, China.

3 Key Laboratory for Agricultural Land Quality, Ministry of Natural Resources of the People's Republic of China, Beijing 100083, China.

*Address correspondence to: zhaoyuanyuan@cau.edu.cn

Abstract: Natural and planted forests differ substantially in ecological functions and economic values, with forest age serving as a key indicator of their developmental and carbon dynamics. However, existing global forest age datasets remain constrained by coarse spatial resolution and the lack of explicit forest type distinction. In this study, we developed a 30 m global forest age dataset for 1985–2024 by integrating Landsat time-series data with the Continuous Change Detection and Classification (CCDC) algorithm on the Google Earth Engine platform, thereby reducing reliance on ground-based forest inventory data. Building upon global forest distribution products, forest age was estimated from change points in long-term spectral trajectories, distinguishing the age of natural and planted forests at a global scale. Validation using 6,100 globally stratified samples demonstrated strong agreement with visually interpreted references (overall accuracy = 0.72, RMSE = 5.66 years), with higher accuracy for natural forests (0.73) than for planted forests (0.70). Globally, pronounced regional contrasts were observed: old-growth native forests (NF) dominate in Europe (84.38%), South America (82.61%), and North America (80.62%), whereas Australia exhibits a bimodal age distribution driven by both old and regenerating stands. Planted forests (PF), by contrast, are consistently younger, with the youngest plantations concentrated in Australia (Age1–5: 65.77%) and the most mature in Europe (Age36–40: 53.99%). This 30 m global forest age map provides a consistent and high-resolution benchmark for improving forest carbon accounting, plantation yield modeling, and conservation strategy development.

1 Introduction

Forests represent one of the most vital ecosystems on Earth, covering approximately 31% of the global land surface and providing habitats for most terrestrial species (FAO 2024). They play a central role in regulating the global carbon cycle,

https://doi.org/10.5194/essd-2025-674
Preprint. Discussion started: 8 January 2026

storing nearly 296 billion tons of carbon and contributing to climate stability, hydrological balance, and biodiversity conservation (FAO 2024; Murphy et al., 2025; Noss 1999; Thompson et al., 2009). Beyond ecological functions, forests supply wood, fiber, fuel, and food, supporting the livelihoods of billions of people worldwide (Oldekop et al., 2020; Steel et al., 2024). In the context of accelerating climate change and global sustainability challenges, understanding forest structure and dynamics—especially forest age—has become indispensable for assessing carbon sequestration potential, guiding restoration efforts, and ensuring long-term ecological and social resilience (Erdozain et al., 2024; Leng et al., 2024; Tian et al., 2024; Zhang et al., 2023).

Stand age represents one of the most critical dimensions differentiating NF and PF in terms of growth characteristics and carbon sequestration capacity (Köhl et al., 2017; Liang et al., 2022). PF typically exhibit uniform age structures, with vegetation and soil carbon storage increasing continuously with age. However, their total carbon accumulation is generally lower and highly dependent on management regimes (Cao et al., 2025; Zou et al., 2023). In contrast, NF possess longer growth cycles and complex age distributions; their carbon sequestration rate tends to stabilize after maturity, resulting in higher total carbon stocks and richer ecosystem functions (He et al., 2022; Liang et al., 2022; Liao et al., 2023; Shi et al., 2022). These divergent age–carbon relationships introduce significant uncertainties in carbon sink estimation when using models such as the Integrated Terrestrial Ecosystem C-budget (InTEC) model (Chen et al., 2000). Accurate information on both forest type and age is therefore essential for improving carbon accounting precision and guiding evidence-based forest management (Cheng et al., 2024; Mo et al., 2024). To fully assess the contribution of both forest types to climate mitigation and biodiversity conservation, mapping their age distributions at the global scale is of paramount importance (Aszalós et al., 2022).

Currently, five primary approaches are employed to estimate forest age using remote sensing: statistical models, image classification, remote sensing inversion of forest parameters, multi-sensor data fusion and time-series change detection. Statistical models, such as multiple linear regression and machine learning algorithms (e.g., Random Forests and Support Vector Machines), estimate forest age based on biophysical variables. However, these models are often constrained by their limited ability to capture complex nonlinear relationships. Image classification approaches infer age from spectral reflectance and vegetation indices, though their accuracy decreases with finer age stratification or heterogeneous species composition (Reyes-Palomeque et al., 2021). Remote sensing inversion methods, including K-Nearest Neighbor and Random Forest regression, can capture nonlinear relationships but remain vulnerable to overfitting when applied across diverse ecosystems (Tang et al., 2020). In addition to optical data, synthetic aperture radar (SAR) and LiDAR observations have demonstrated strong potential for forest age estimation. SAR systems, such as ALOS PALSAR and Sentinel-1, are sensitive to canopy structure and moisture content, enabling effective forest monitoring under persistent cloud cover and alleviating the spectral saturation issues commonly observed in optical indices (Champion et al., 2013; Trisasongko et al., 2020). However, SAR backscatter tends to saturate in high-biomass forests and is strongly influenced by terrain, soil moisture, and incidence angle, which complicates its interpretation. Moreover, the relatively coarse resolution of global SAR products limits their ability to detect fine-scale age variations. LiDAR, on the other hand, directly captures the three-dimensional forest structure—such as canopy height and vertical distribution—providing critical parameters for calibrating age–height models (Racine et al., 2014).

https://doi.org/10.5194/essd-2025-674
Preprint. Discussion started: 8 January 2026

Nevertheless, LiDAR data suffer from sparse spatial coverage, high acquisition costs, and poor temporal consistency, which restrict their applicability for large-scale or long-term forest age monitoring. More recently, with the open availability of Landsat data, time-series algorithms such as LandTrendr and CCDC have achieved remarkable progress in forest age estimation and regional mapping. These approaches analyze temporal trajectories of spectral reflectance or vegetation indices to track gradual or abrupt pixel-level changes, identify disturbance and recovery processes, and thereby infer forest establishment time and subsequent growth stages (Du et al., 2022; Li et al., 2024; Xiao et al., 2023).

Many forest age products have been developed based on these approaches, yet only a few products provide global-scale coverage. Below are key representatives of such global products: The Global Forest Age Dataset (GFAD) describes age distributions of plant functional types on a 0.5 ° grid for the period 2000–2010, derived from inventory data in temperate and boreal regions and biomass–age relationships in tropical areas (Poulter et al., 2018). Besnard et al. (2021) produced a circa 2010 global forest age dataset at 1 km resolution by integrating forest inventory, biomass, and climatic data. This product was later updated to the Global Age Mapping Integration (GAMI) at a resolution of 100 m (Besnard et al., 2024). More recently, Du et al. (2022) created a 30 m-resolution global dataset of planting years of plantation (PYP) based on Landsat time-series analysis, offering higher spatial detail but focusing solely on planted forests.

Despite the respective advantages of these approaches—statistical and inversion models offering local-scale precision, image classification enabling rapid mapping over small areas, and time-series algorithms providing large-scale temporal continuity—current forest age products still face major limitations. First, most large-scale datasets lack the spatial resolution needed to capture fine-scale age heterogeneity (Smolina et al., 2023). Second, they seldom differentiate between NF and PF, undermining the reliability of carbon sequestration estimates given their contrasting age–carbon trajectories (Su et al., 2023; Yu et al., 2024). Third, many products remain confined to specific regions or forest types, limiting their global applicability (Besnard et al., 2021; Huang et al., 2023; Lu et al., 2025; Maza et al., 2021). These limitations highlight the urgent need for high-resolution, globally consistent forest age mapping that distinguishes between NF and PF. Thus, a comprehensive global forest age dataset integrating high spatial resolution, explicit forest type differentiation, and worldwide coverage remains absent. Developing such a dataset is crucial for enhancing global carbon stock quantification and improving forest-based climate mitigation assessments.

To address this gap, we applied the CCDC algorithm within the Google Earth Engine (GEE) environment to estimate forest age for both NF and PF using Landsat 4–8 surface reflectance data from 1985–2024. Based on the Global Natural and Planted Forests (GNPF) dataset, NF and PF masks were first generated to delineate the spatial extent of each forest type (Xiao et al., 2024). Temporal trajectories within these masks were then modeled using CCDC to derive forest age at 30 m resolution. The resulting global forest age map—the first to distinguish NF and PF at high spatial resolution—has been made publicly available, providing a robust foundation for global research on forest dynamics, carbon storage, and sustainable management.

https://doi.org/10.5194/essd-2025-674
Preprint. Discussion started: 8 January 2026

Open Access Earth System Science Data Discussions

2 Datasets and methods

The workflow of this study includes four main stages (Fig. 1). First, time-series Landsat optical imagery from 1985 to 2024 was preprocessed and reconstructed using the GEE platform. Second, the CCDC algorithm was applied to extract spatiotemporal spectral trajectories and detect forest disturbances and recovery events. Third, the GNPF dataset was used to delineate natural and planted forest areas. Finally, forest age for each forest type was estimated based on CCDC-derived temporal parameters.

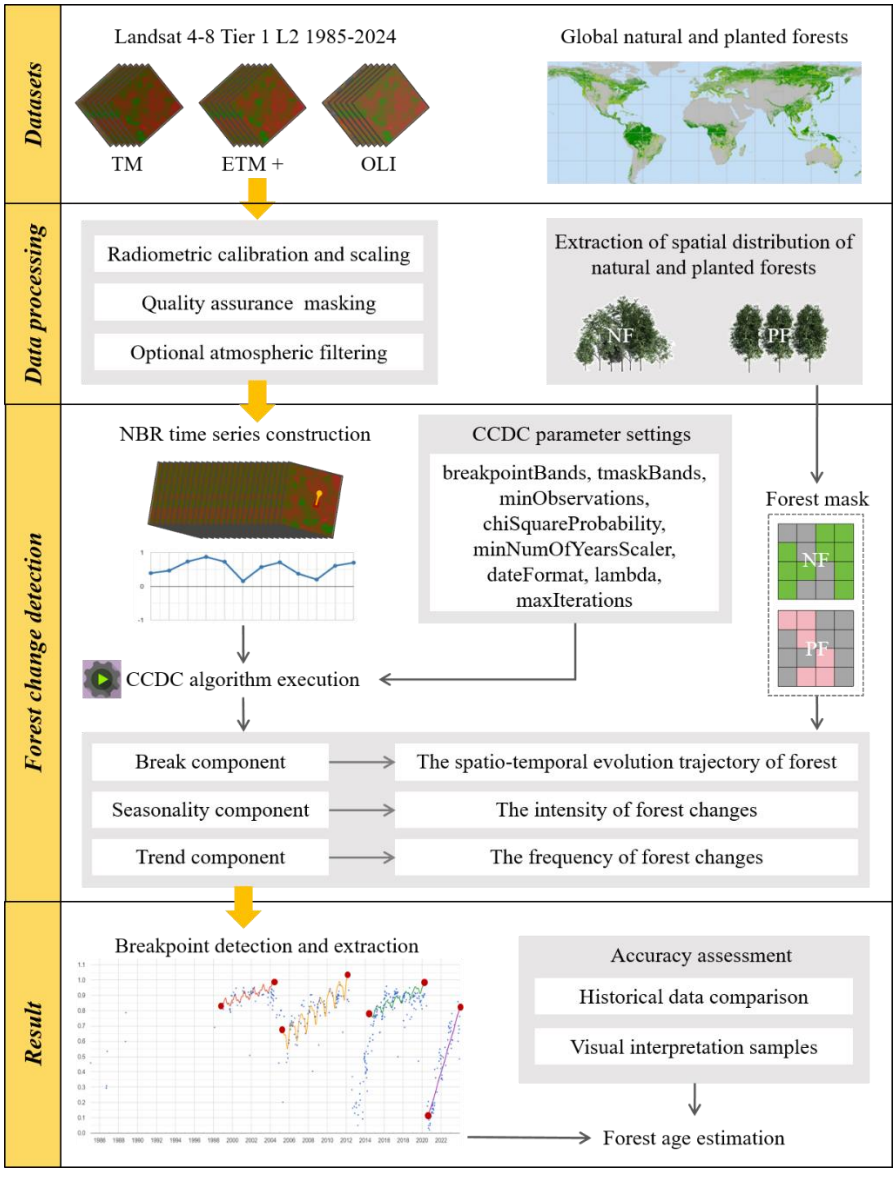

Figure 1: Workflow of estimating forest age for global natural and planted forests.

https://doi.org/10.5194/essd-2025-674
Preprint. Discussion started: 8 January 2026

2.1 Global natural and planted forests dataset

The Global Natural and Planted Forests (GNPF) dataset provides the global distribution of natural and planted forests at 30 m spatial resolution for 2021 (Xiao et al., 2024). Derived from Landsat time-series imagery (1985–2021), the dataset distinguishes forest types based on differences in disturbance frequency, achieving an overall accuracy of 85%. The proportions of forest types are consistent with the FAO's Global Forest Resources Assessment 2020, ensuring high thematic reliability. The GNPF dataset was used to generate a forest type mask that separates natural and planted forest pixels. This mask served as a spatial reference for forest age estimation, enabling independent analysis of temporal dynamics for each forest type.

2.2 Time series construction

All Tier 1 Level-2 surface reflectance products from Landsat 4–8 (TM, ETM+, and OLI sensors) were utilized for the 1985–2024 period. Preprocessing followed the LEDAPS and LaSRC algorithms for radiometric calibration and atmospheric correction (Ju et al., 2012; Vermote et al., 2018). Pixel-level filtering was performed using the QA_PIXEL band to remove clouds, cloud shadows, and saturated pixels. Additional filtering based on aerosol optical depth further improved data quality. To ensure radiometric consistency across sensors, Landsat 8 reflectance values were normalized to match those of ETM+. Several spectral indices were computed for each image, forming a continuous temporal dataset. This stack was analyzed using the CCDC algorithm (Zhu et al., 2014) , with the Normalized Burn Ratio (NBR) serving as the primary variable for disturbance detection and forest age estimation. The final outputs were exported as 30 m raster layers.

2.3 Vegetation index and parameters selection

Vegetation indices provide sensitive indicators of canopy condition and ecosystem dynamics. Among them, the Normalized Burn Ratio (NBR) was selected for this study due to its high responsiveness to vegetation disturbance and recovery. NBR, calculated from the Near-Infrared (NIR) and Shortwave Infrared (SWIR2) bands, effectively captures structural and moisture changes in vegetation, making it particularly suitable for detecting forest loss and regrowth following disturbances such as fire or logging (Bright et al., 2019; Escuin et al., 2008; Ryu et al., 2018). Within the CCDC framework, temporal NBR trajectories were analyzed to identify disturbance and recovery events, enabling precise estimation of forest stand age.

$$NBR=\frac{NIR-SWIR2}{NIR+SWIR2}, \quad (1)$$

2.4 Forest age detection

2.4.1 CCDC algorithm

The CCDC algorithm, implemented on the GEE platform, was used to estimate forest age for both natural and planted forests. CCDC continuously monitors land surface dynamics by analyzing dense time-series satellite imagery at the pixel level. The

https://doi.org/10.5194/essd-2025-674
Preprint. Discussion started: 8 January 2026

algorithm constructs temporal-spectral models for each pixel and identifies structural changes in reflectance patterns over time. In this study, CCDC was applied following three major steps: (1) Model construction: For each pixel, a harmonic regression model incorporating trend and seasonal terms was fitted using ordinary least squares (OLS), producing a continuous spectral trajectory. (2) Change detection: Model predictions were compared with observed values to identify significant deviations. A land cover change was confirmed when three consecutive observations deviated beyond a predefined threshold. (3) Model updating: Once a change was detected, the model was dynamically recalibrated to represent the new surface condition. The main parameters used in the CCDC algorithm are summarized in Table 1. Using the NBR time series from 1985 to 2024 as input, CCDC generated multiple outputs, including breakpoint characteristics (start time, end time, breakpoint time, number of valid observations, and change probability), as well as segment-level parameters (regression coefficients, RMSE, and the maximum normalized residual at breakpoints).

$$\hat{\rho}(i,x) = a_{0,i} + a_{1,i}\cos\frac{2\pi x}{T} + b_{1,i}\sin\frac{2\pi x}{T} + a_{2,i}\cos\frac{2\pi x}{NT} + b_{2,i}\sin\frac{2\pi x}{NT} \quad (2)$$

In the Eq. (2), $\hat{\rho}(i,x)$ represents the predicted value of the i-th band of fitted Julian date x; i represents the i-th spectral band; T represents the number of days in each year; $a_{0,i}$ represents the total value of the i-th band reflectance; $a_{1,i}$ and $b_{1,i}$ represent the coefficient of the intra-annual variation term of the reflectance of the i-th band; $a_{2,i}$ and $b_{2,i}$ represent coefficients for inter-annual change for the i-th band; N represents number of years.

Table 1. Parameter settings for CCDC in this study.

Input	Parameters
breakpointBands	'GREEN', 'RED', 'NIR', 'SWIR1', 'SWIR2','NBR'
tmaskBands	'GREEN', 'SWIR2'
minObservations	6
chiSquareProbability	0.99
minNumOfYearsScaler	1.33
dateFormat	1
lambda	0.002
maxIterations	10000

2.4.2 Forest age identification based on breakpoints

The CCDC-derived pixel-level temporal trajectories were used to identify and quantify forest growth cycles. Each fitted time series was decomposed into discrete temporal segments bounded by breakpoints, which correspond to abrupt land cover transitions such as afforestation, harvesting, or disturbance events (Fig. 2). To estimate current forest age, the latest stable segment—representing the most recent undisturbed growth phase—was extracted for each pixel. The starting year of this final segment was defined as the onset of the current forest growth period, while the study year (2024) was used as the reference

https://doi.org/10.5194/essd-2025-674
Preprint. Discussion started: 8 January 2026

Open Access Earth System Science Data Discussions

endpoint. Forest age was then calculated as the time interval between these two points. This approach effectively captures forest stand age by quantifying the duration since the last major disturbance or establishment event.

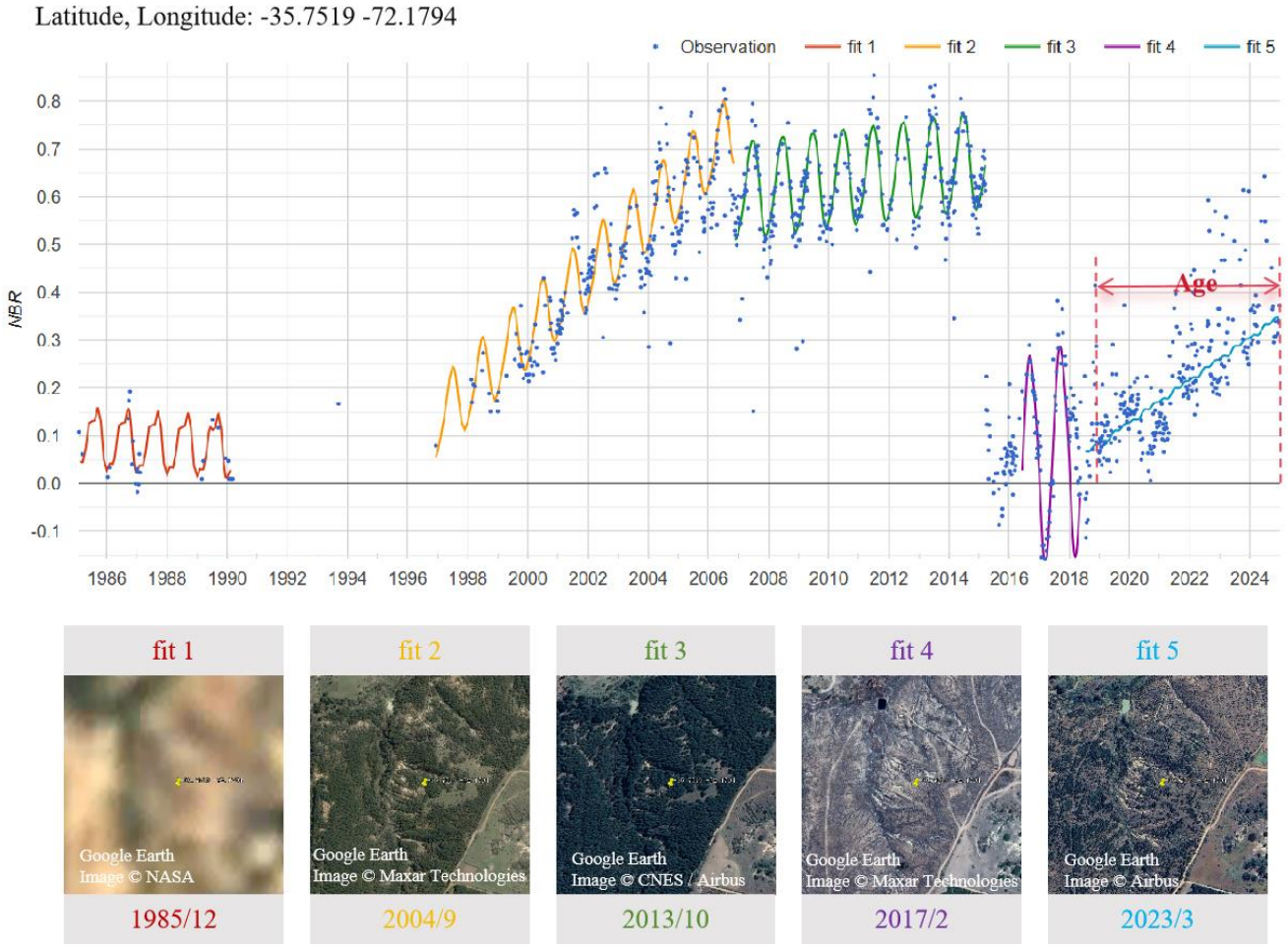

Figure 2: Forest age determination based on time-series breakpoints. This figure illustrates the time-series fitting results for a single pixel and the corresponding remote sensing images for each fitted segment. Among these segments, the last segment (labeled as "fit5") is identified as the target segment, as it represents the latest growth stage following the most recent disturbance. The time span of this target segment (i.e., the duration from the start year to the end year of fit5) directly corresponds to the forest age.

2.4.3 Adaptive grid partitioning across global continents

To ensure computational efficiency and facilitate large-scale processing, an adaptive grid partitioning scheme was developed based on the Large Scale International Boundary (LSIB) dataset from the U.S. Department of State's Office of the Geographer and Global Positioning Systems (2017). The dataset, which integrates and simplifies global administrative boundaries while maintaining essential regional distinctions, provides sufficient spatial precision for continental-scale analysis. Using the "Continental Region" layer of the LSIB, the global landmass was divided into spatial units for independent CCDC processing.

https://doi.org/10.5194/essd-2025-674
Preprint. Discussion started: 8 January 2026


Open Access Earth System Science Data Discussions

As the GNPF dataset did not predict any forest cover in the South Atlantic, Antarctica, and Greenland (within the North American region), these areas were excluded from subsequent analyses. This exclusion reduced computational redundancy and prevented interference from invalid grids, thereby enhancing global processing efficiency.

2.5 Validation samples generation using GNPF and high-resolution imagery

To rigorously evaluate the accuracy of forest age estimates derived from the CCDC algorithm, we established a validation framework based on three key principles: (1) consistency with benchmark datasets, (2) spatial representativeness of validation samples, and (3) verification using high-resolution imagery (Fig. 3). First, to ensure alignment with the spatial scale of the GNPF product, the global land surface was divided into 57,559 independent $0.5° \times 0.5°$ grid cells. This partitioning provided a uniform spatial framework for sample selection and validation. Second, within each grid, stratified random sampling was performed based on the GNPF-derived forest type classification ("natural forest" and "planted forest"). For each forest type, five samples were randomly selected per grid, while grids lacking forest cover were excluded. This grid-based, forest type–stratified sampling strategy ensured balanced representation between natural and planted forests and avoided spatial clustering of validation samples, thereby achieving global spatial uniformity. Finally, reference forest ages were determined through manual interpretation of historical high-resolution imagery available in Google Earth. The initial establishment or regeneration year of each forest stand was visually identified by examining multi-temporal image sequences, which marks the onset of the forest's current growth cycle. These visually interpreted reference ages were then compared with the CCDC-derived estimates on a per-sample basis to assess the algorithm's performance for both NF and PF.

https://doi.org/10.5194/essd-2025-674
Preprint. Discussion started: 8 January 2026

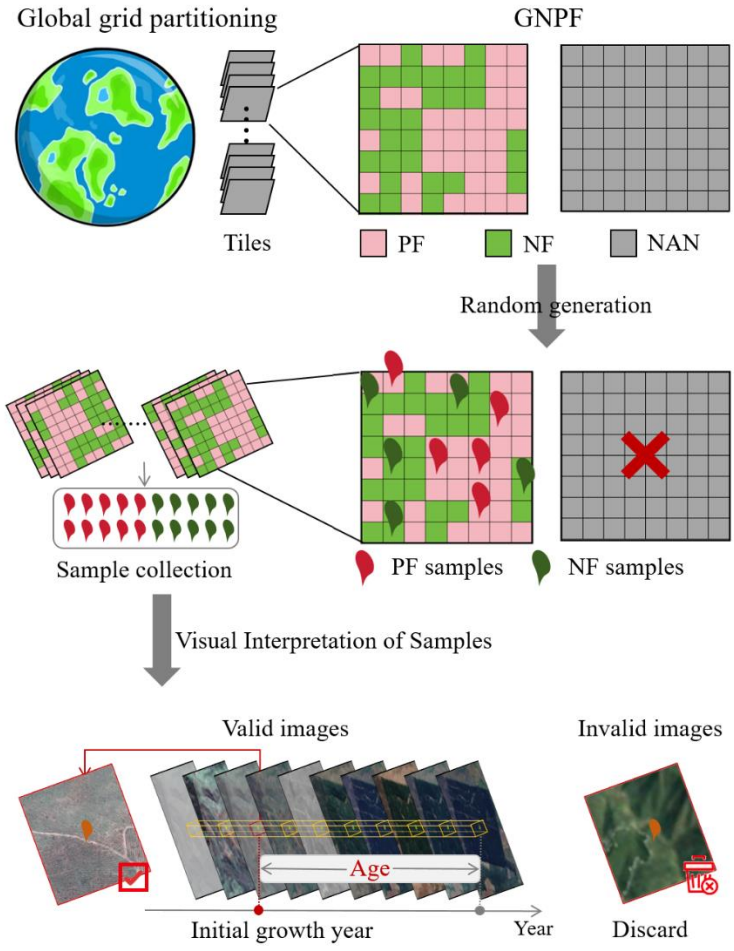

Figure 3: Workflow for generating validation samples using global grid-based stratified sampling.

3 Results

3.1 Forest age accuracy

3.1.1 Validation using independently interpreted samples

To comprehensively evaluate the accuracy of forest age estimation, a total of 6,100 globally stratified validation samples were collected, including 3,065 from PF and 3,035 from NF (Fig. 4a). Model-predicted forest ages were compared with visually interpreted reference ages. As shown in Figure 4b, the observed and predicted forest ages exhibited a strong linear relationship, indicating that the model effectively captured the temporal variation in forest age. The root mean square error (RMSE = 5.66) suggests that the average deviation between predicted and observed values was within an acceptable range. Figure 4c further compares the prediction accuracy of NF, PF, and the combined dataset (ALL) under different error tolerance thresholds.

https://doi.org/10.5194/essd-2025-674
Preprint. Discussion started: 8 January 2026

Open Access Earth System Science Data Discussions

Overall, under the strictest evaluation criterion (0-year tolerance), the model achieved an accuracy of 0.73 for NF, 0.70 for PF, and 0.72 overall, indicating strong agreement even under exact matching conditions. When the tolerance expanded to ±5 years, accuracies increased markedly to 0.95 for NF, 0.87 for PF, and 0.91 overall (Fig. 4c). The consistently higher performance for NF highlights the model's superior capability in capturing the temporal dynamics of NF. These results confirm that the CCDC-based approach provides reliable forest age estimates globally, with particularly high robustness under reasonable tolerance thresholds.

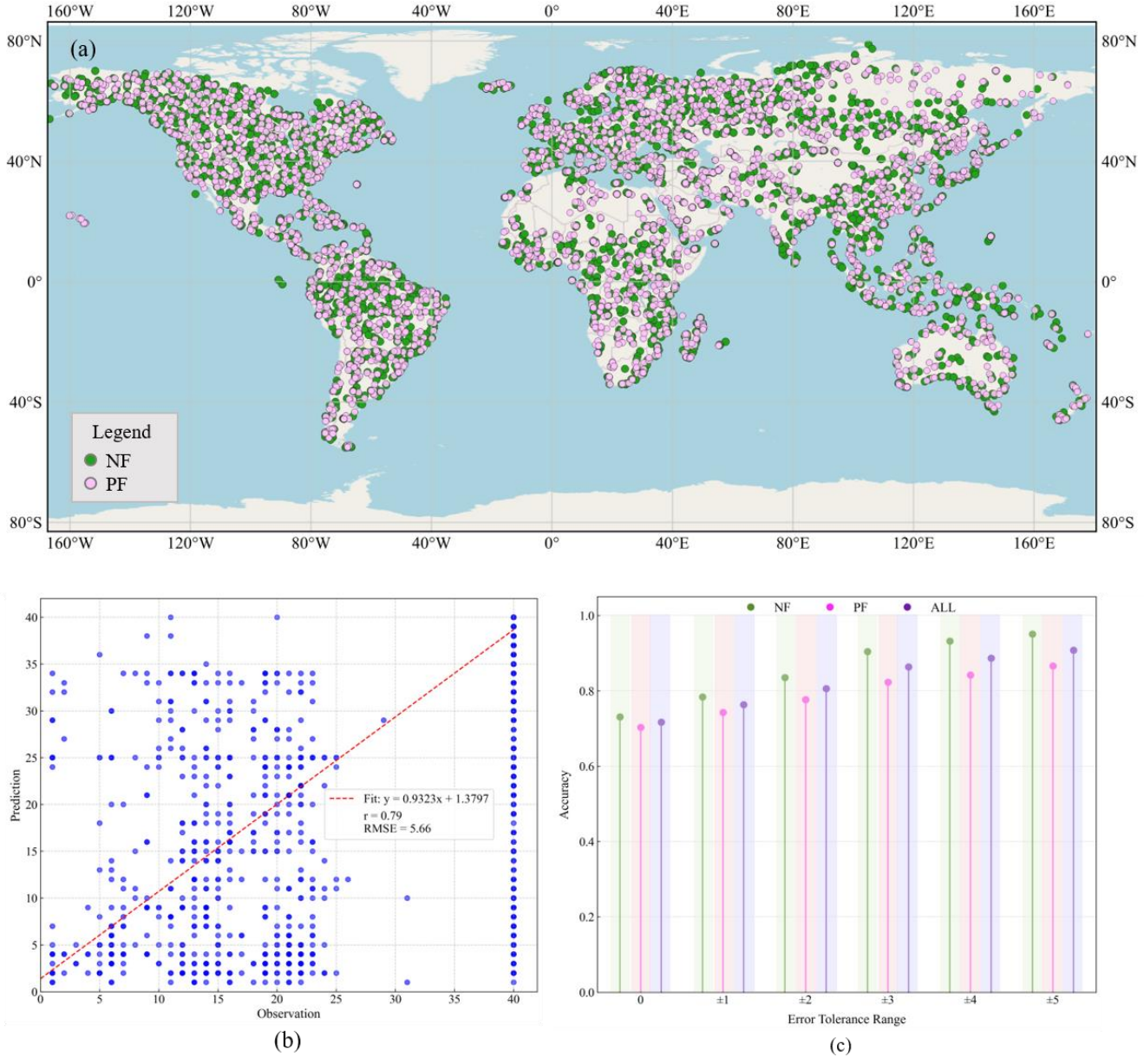

https://doi.org/10.5194/essd-2025-674
Preprint. Discussion started: 8 January 2026

Figure 4: Validation sample distribution and accuracy verification of forest age prediction model. (a) The global distribution of validation samples. (b) Scatter plot and fitting relationship between observed and predicted forest ages. (c) Comparison of forest age prediction accuracy among different forest types under various error tolerance ranges. NF represents natural forest, PF represents planted forest, and ALL represents the combination of the two types of forests.

3.1.2 Comparison with existing products

To assess the reliability of the forest age estimates, we compared our product—the Global 30m Forest Age Map (Natural vs. Planted) (GFAM-N/P)—with a 30 m-resolution forest age product (FAP) developed by Xiao et al. for China (2023). The reference dataset identifies forest establishment years from 1990 to 2020, whereas our study extends the temporal coverage to 1985–2024. Despite this difference, both datasets exhibited strong agreement in forest age estimation within the overlapping period.

To ensure fair comparison, we performed stratified random sampling within the overlapping forested area based on China's climatic regionalization (Fig. 5a). Specifically, 100 samples were selected from each of the tropical monsoon, temperate continental, and alpine plateau climatic zones, and 200 samples from each of the subtropical monsoon and temperate monsoon zones, resulting in 700 uniformly distributed samples across the country (Fig. 5b). Differences in forest age between the two datasets were analyzed using both a difference histogram and Bland–Altman consistency analysis (Bunce 2009). The results showed that the age differences were narrowly distributed and symmetrically centered around 0 (Fig. 5c). The kernel density estimation (KDE) curve displayed a sharp and narrow peak (Terrell et al., 1992), indicating that most samples had minimal deviations in forest age. In the Bland–Altman plot, the mean difference (red dashed line) was close to 0, and 95% of the samples fell within the consistency limits, with only a few isolated outliers (Fig. 5d). These findings demonstrate a high level of consistency between the two products, suggesting that despite differences in temporal span, both share similar methodological logic in forest age extraction and produce comparable results during the overlapping period.

https://doi.org/10.5194/essd-2025-674
Preprint. Discussion started: 8 January 2026

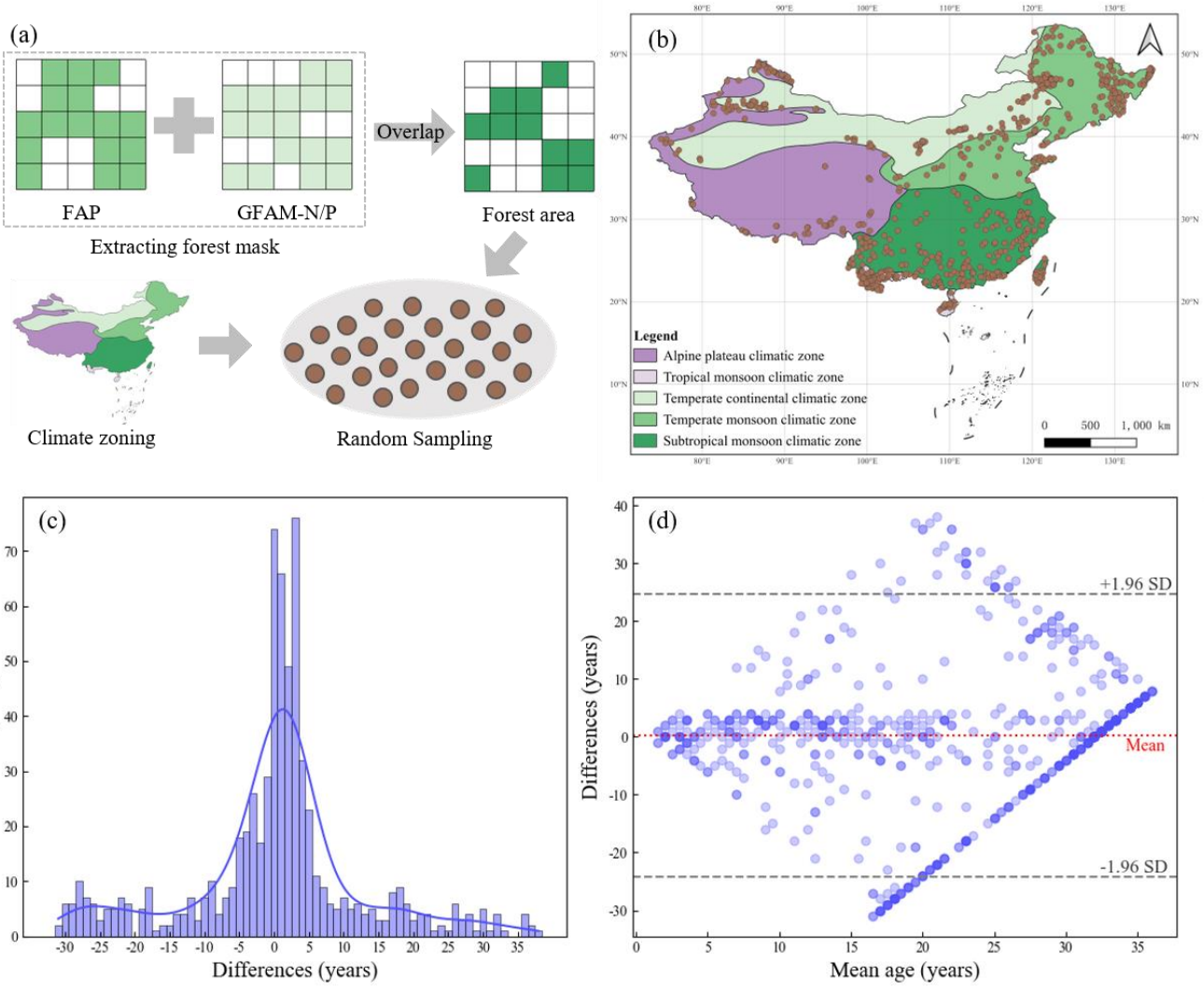

Figure 5: Sample generation, distribution and accuracy assessment. (a) Sample generation. (b) Spatial distribution of samples across climatic zones in China. (c) Distribution of forest age differences between the GFAM-N/P and the FAP (difference = GFAM-N/P − FAP). (d) Bland–Altman plot showing the agreement between the two datasets; the central red line represents the mean difference (bias), and the gray dashed lines indicate the ±1.96 × standard deviation range (95% limits of agreement).

We conducted a visual comparison between the GFAM-N/P and the GAMI dataset developed by Besnard et al., (2024) , which has a spatial resolution of 100 m. Figure 6 presents three representative comparison sites that highlight differences in spatial detail and data quality. At Site 1, the GFAM-N/P revealed finer and more continuous gradients in forest age. In contrast, the coarser 100 m resolution of GAMI limited its ability to capture small and fragmented forest patches, leading to partial or missing age information. At Site 2, where forests dominated the landscape, GAMI failed to delineate forest age in large areas. This omission can be attributed not only to its lower spatial resolution but also to its data fusion approach, which likely removed pixels with low inter-source consistency, thereby reducing fine-scale structural details. At Site 3, GAMI depicted only

https://doi.org/10.5194/essd-2025-674
Preprint. Discussion started: 8 January 2026

fragmentary forest age patterns, again reflecting limitations associated with its empirical modeling framework. Because the GAMI dataset estimates forest age from the empirical relationship between biomass and stand age, its accuracy is inherently constrained by input data quality and model assumptions. In contrast, the GFAM-N/P captures spatiotemporal variations in both planted and natural forests at a finer spatial resolution, providing enhanced insights into forest growth dynamics and carbon sequestration potential. This improvement underscores the value of our dataset for precision forest management and carbon cycle monitoring at regional and global scales.

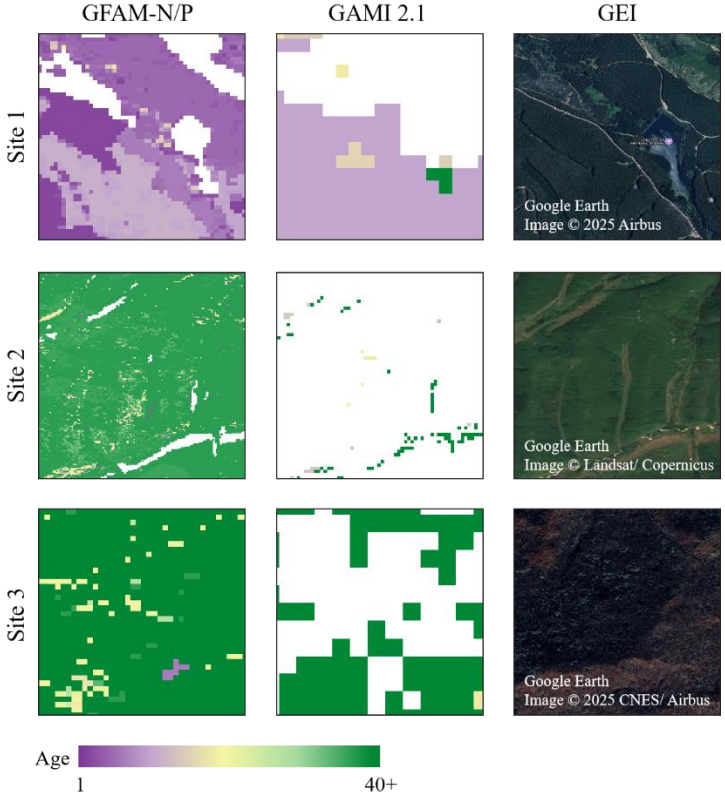

Figure 6: Comparison between the GFAM-N/P and the 100 m-resolution GAMI 2.1 product across three representative sites. White pixels in the forest age maps represent non-forest areas.

3.2 Global forest age spatial distribution characteristics

Globally, forest age exhibits distinct spatial patterns between NF and PF (Fig. 7). NF are broadly distributed across tropical, subtropical, and boreal regions, with older stands concentrated in the Amazon Basin, Central Africa, and northern Eurasia. These mature forests largely correspond to areas with minimal anthropogenic disturbance and long-term ecological stability. In contrast, PF are mainly distributed in the mid-latitudes, including East Asia, Europe, Australia, and southeastern South America, reflecting intensive forest management and large-scale reforestation efforts over recent decades (Bennett 2015). The global map reveals a clear latitudinal gradient: younger forests dominate economically developed and actively managed

https://doi.org/10.5194/essd-2025-674
Preprint. Discussion started: 8 January 2026

regions (e.g., East Asia, Europe, and parts of North America), while older stands prevail in equatorial and high-latitude zones. Compared with NF, PF exhibit a markedly younger age structure worldwide. Most PF areas fall within the 1–15-year range, particularly in China, Brazil, and the southeastern United States, where short-rotation plantation systems are common. In contrast, NF contain a substantially higher proportion of mature stands (>30 years), especially in remote tropical and boreal zones dominated by natural succession. These spatial contrasts primarily stem from differences in forest management intensity, reforestation policies, and disturbance regimes. Younger PF ages in subtropical and temperate regions correspond to large-scale plantation rotations, whereas older NF ages in tropical and boreal areas reflect long-term ecological continuity. Compared with existing coarse-resolution products such as GAMI (100 m), the 30 m forest age map developed in this study provides a more detailed representation of spatial heterogeneity and better captures fine-scale age gradients across fragmented landscapes.

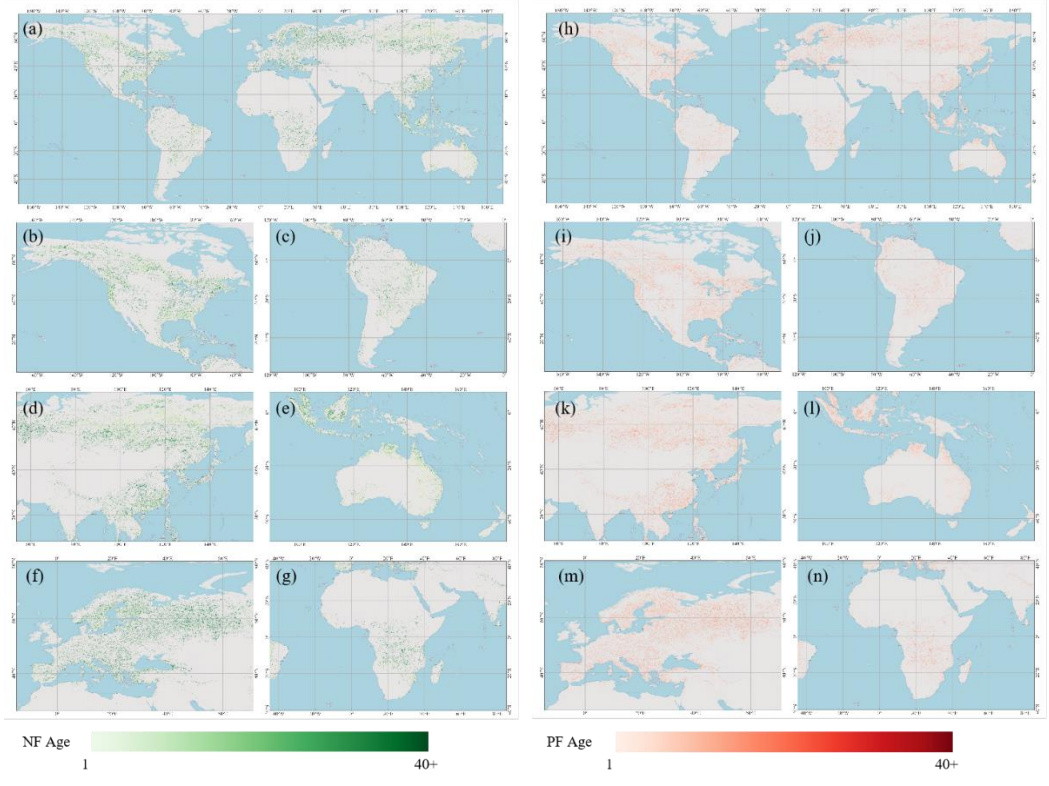

Figure 7: The distribution of global forest age. Natural forests (left) and planted forests (right). (a) presents the global spatial pattern of NF ages, with zoomed-in views of key regions including North America (b), South America (c), Asia (d), Australia (e), Europe (f), and Africa (g); (h) displays the global distribution of PF ages, complemented by zoomed-in views of North America (i), South America (j), Asia (k), Australia (l), Europe (m), and Africa (n).

https://doi.org/10.5194/essd-2025-674
Preprint. Discussion started: 8 January 2026

3.3 Regional variations in age structure between planted and natural forests

Building upon the global spatial distribution patterns, we further quantified regional variations in the age structure of NF and PF across six continents—Africa, Asia, Australia, Europe, North America, and South America—to reveal their distinct developmental characteristics and management contexts.

The age structures of NF and PF exhibit pronounced regional contrasts (Fig. 8). For NF, Europe (84.38%), South America (82.61%), and North America (80.62%) show a predominance of the oldest age class (Age36–40), each typically exceeding 80%. Africa (66.46%) and Asia (48.61%) follow this pattern, whereas Australia exhibits a notable bimodal pattern, with both young (Age1–5: 31.36%) and old (Age36–40: 35.64%) stands contributing substantially. Except for Australia, young NF (Age1–10) occupy less than 8% across all other continents. Notably, Asia contains a relatively high proportion of middle-aged forests (Age21–25: 21.95%), suggesting more active regeneration and a balanced age composition. PF, in contrast, are markedly younger across all continents. In Australia, PF are highly concentrated in the youngest class (Age1–5: 65.77%), with only 8.12% in the oldest (Age36–40). The young age structure is likely associated with the dominance of short-rotation species widely used in Australian plantations (Strandgard et al., 2021). Both Africa and South America exhibit a "young-and-old dual peak" structure—Africa (Age1–5: 31.09%; Age36–40: 36.60%) and South America (Age1–5: 31.11%; Age36–40: 32.59%). PF in North America (Age1–5: 17.66%) and Asia (Age1–5: 18.58%) are generally skewed toward younger stands, though older classes still represent 34.36% and 30.09%, respectively. Europe is the only region where old PF dominate (Age36–40: 53.99%), while young PF remain below 20%. Regionally, PF in Australia, Asia, and North America are dominated by younger stands, Africa and South America exhibit mixed age compositions, and Europe is characterized by relatively mature plantation structures.

https://doi.org/10.5194/essd-2025-674
Preprint. Discussion started: 8 January 2026

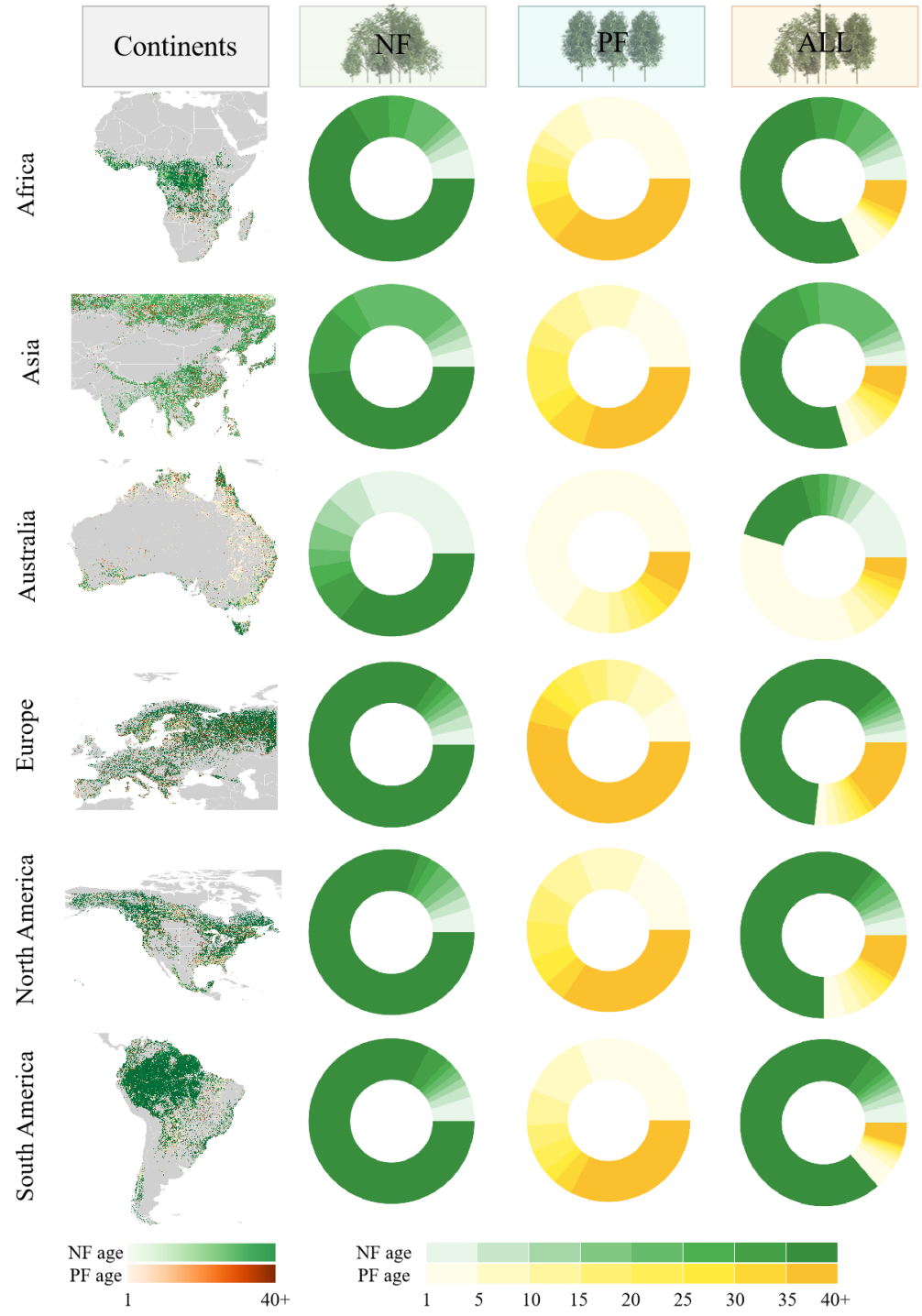

290 **Figure 8: Regional age-class distributions of planted and natural forests across six continents. The first column shows the six global regions. The second and third columns depict the proportional distributions of NF and PF, respectively, across eight age classes (1–5 to 36–40 years, in 5-year intervals). The fourth column summarizes the total proportions of NF and PF within each region.**

https://doi.org/10.5194/essd-2025-674
Preprint. Discussion started: 8 January 2026

4 Discussion

4.1 Advances in existing forest age products

Current global forest age products—such as GFAD, GAMI and PYP —face inherent limitations in spatial resolution, regional adaptability, and the differentiation of NF and PF. Most existing datasets operate at coarse spatial resolutions (≥100 m) or limited regional scales and typically do not distinguish forest origin, leading to mixed and often biased age estimates that obscure management-driven differences in forest dynamics. The 30 m GFAM-N/P developed in this study addresses these challenges by offering spatially explicit and origin-specific age estimates for NF and PF. This fine spatial detail enables the detection of subtle regional variations in age structure, particularly across heterogeneous landscapes in Asia and South America where natural and planted forests are closely interwoven. These technical advances are pivotal because they resolve the long-standing inability of coarse-resolution products to capture the fine-scale dynamics of forest age—dynamics that underpin critical processes like carbon sequestration and biodiversity maintenance. Comparative analyses with existing products (Fig. 9) highlight these improvements: our dataset captures fine-scale gradients absent from coarser products such as GAMI and PYP, while the latter shows data gaps across regions like South America and Europe due to limited plantation records. Forest origin classification in this study was derived from the GNPF 2022 dataset, with minimal conversion assumed between 2022 and 2024. Nevertheless, post-2022 disturbances—such as harvesting or deforestation—may introduce localized inconsistencies in age estimation.

https://doi.org/10.5194/essd-2025-674
Preprint. Discussion started: 8 January 2026

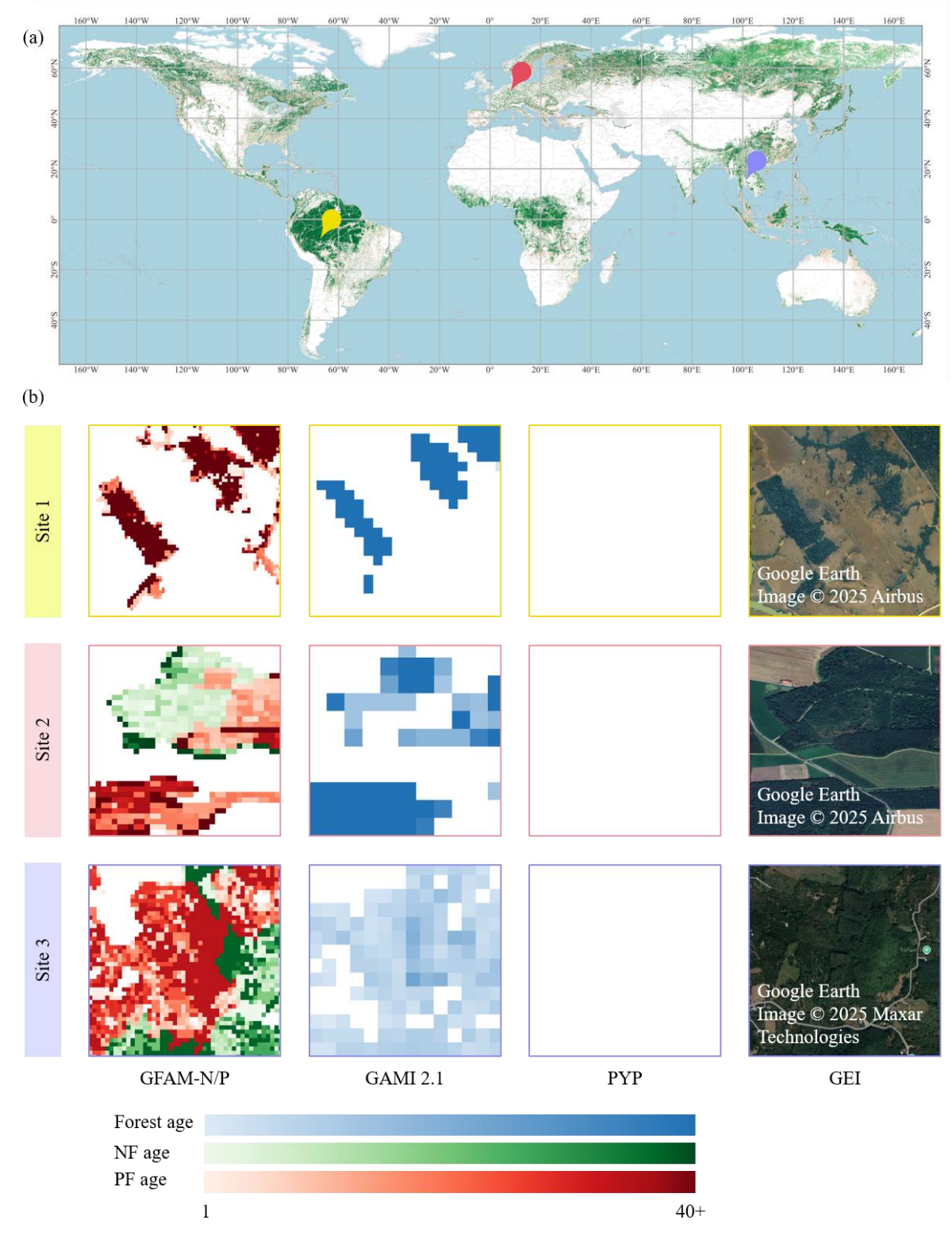

https://doi.org/10.5194/essd-2025-674
Preprint. Discussion started: 8 January 2026

Figure 9: Comparison of global forest age products and demonstration of spatial improvements achieved in this study. (a) Global distribution of three representative validation sites used for product comparison. (b) Local comparisons among the GFAM-N/P, the GAMI 2.1 product, the planting year of plantations (PYP) dataset, and high-resolution Google Earth Imagery (GEI). The three sites represent heterogeneous forest landscapes across South America (Site 1), Europe (Site 2), and Southeast Asia (Site 3). Blank regions in the PYP column indicate areas with no available data.

4.2 Regional differences and management implications

Regionally, the age structures of NF and PF exhibit pronounced spatial contrasts that reflect the interplay of historical legacies, ecological constraints, and socioeconomic drivers (Fig. 10). On average, PF are significantly younger than NF across all regions, with mean ages generally below 30 years, compared with 30–36 years for NF in temperate zones. This divergence highlights the differential impacts of forest management intensity, disturbance frequency, and policy orientation among regions. In Europe, both NF and PF display relatively mature age profiles (35.86 years and 28.46 years, respectively), reflecting long-term forest governance, stable land tenure, and well-established silvicultural practices. In contrast, PF in tropical and subtropical regions, such as Southeast Asia (21.14 years) and Africa (21.66 years), are notably younger, consistent with rapid plantation expansion and short-rotation management for timber or agroforestry production. Australia represents an extreme case, where PF average only 9.44 years, underscoring the dominance of fast-growing exotic species under intensive cultivation systems. For NF, regional variability is less pronounced. The oldest stands occur in Europe (35.86 years) and South America (35.18 years), where extensive old-growth and late-successional forests persist under conservation-oriented frameworks. By contrast, younger NF in South Asia (28.57 years) and Oceania (32.48 years) likely reflect stronger disturbance regimes, ongoing regeneration, or transitional successional dynamics. This regional divergence is not merely a descriptive pattern but a manifestation of the global trade-off between economic development and ecological resilience: mature forests in Europe exemplify long-term stewardship, while young plantations in the tropics reflect urgent resource demands in developing economies. Overall, these spatial patterns suggest that forest age is governed less by biophysical constraints than by management intensity and policy legacies. Promoting extended rotation cycles and adaptive, ecosystem-based management—particularly in tropical Africa, Asia, and Oceania—will be essential for enhancing carbon stability and long-term resilience under accelerating global change.

https://doi.org/10.5194/essd-2025-674
Preprint. Discussion started: 8 January 2026

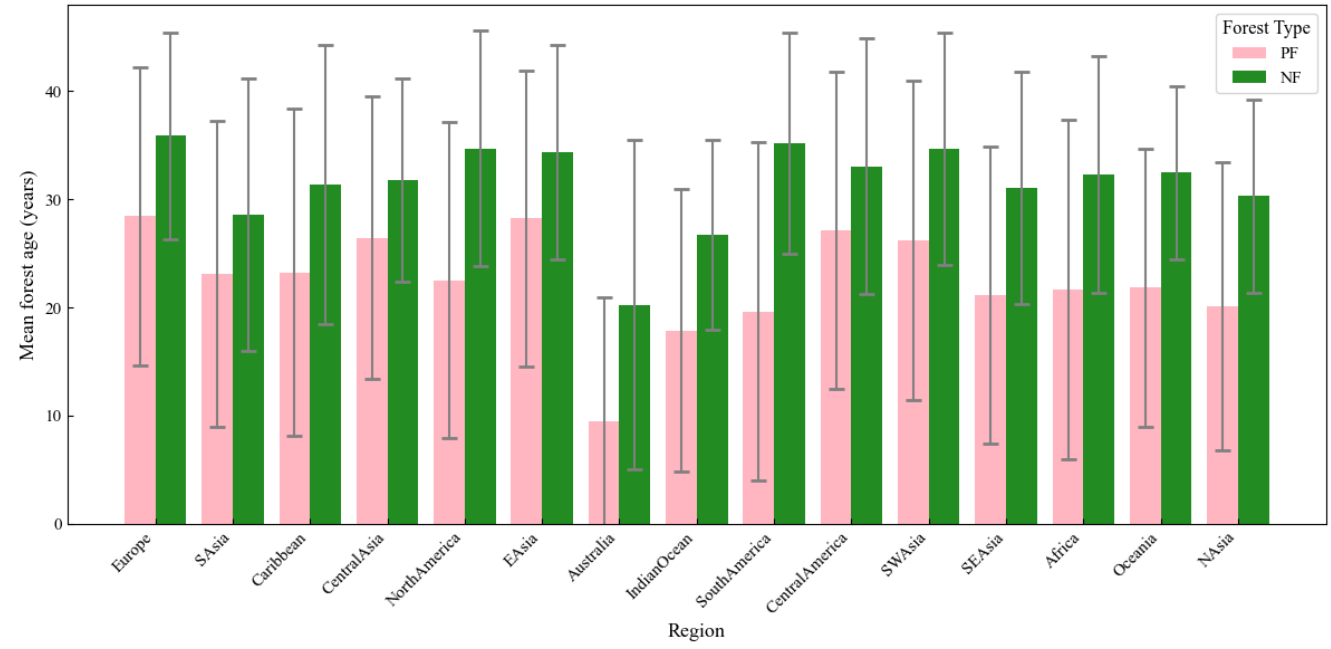

Figure 10: Regional comparison of mean forest age for natural and planted forests. Regional comparison of mean forest age for NF and PF across 15 major biogeographic regions. Bars indicate mean forest age (years), and error bars represent one standard deviation.

4.3 Limitations and scaling potential

Despite the advantages of high-resolution, Landsat-based time-series analysis, several sources of uncertainty remain. Persistent cloud contamination in tropical and humid regions—particularly in Southeast Asia, Central Africa, and the Amazon Basin—can degrade temporal signal quality and obscure subtle disturbance–recovery dynamics. Moreover, radiometric inconsistencies caused by striping artifacts inherent to Landsat imagery may locally distort spectral trajectories, introducing biases in forest age estimation. This issue occurs in African regions, where image banding effects occasionally disrupt the stability of time signals and lead to uncertainty in local estimates. In future work, integrating Sentinel-1 synthetic aperture radar (SAR) time-series data into large-scale forest age estimation frameworks offers a promising pathway to mitigate these limitations by enhancing temporal continuity and improving signal reliability under persistently cloudy conditions. Radar observations are unaffected by cloud cover and capable of capturing canopy structure dynamics, providing complementary information to optical data. The integration of optical and SAR observations will improve temporal continuity, enhance forest change detection accuracy, and strengthen forest age estimation in persistently cloudy tropical regions. For instance, SAR interferometry can quantify canopy height changes, which, when integrated with Landsat-derived leaf area index dynamics, will refine age estimation for young plantations (rotation cycles < 10 years) in cloudy tropical regions. Beyond data-related constraints, the pronounced spatial heterogeneity in forest age structures underscores the necessity of region-specific

https://doi.org/10.5194/essd-2025-674
Preprint. Discussion started: 8 January 2026

management strategies. In short-rotation regions (e.g., Australia, Africa, and parts of Southeast Asia), extending rotation cycles and promoting mixed-species plantations can enhance ecological resilience and long-term carbon sequestration. Conversely, in regions dominated by mature NF (e.g., Europe and North America), management should focus on maintaining natural regeneration, structural diversity, and habitat continuity to sustain biodiversity and carbon stability. Asia, with its relatively balanced forest age composition, represents a transitional system where both protection-oriented and productivity-driven strategies can coexist. Ultimately, the global differentiation of NF and PF age structures revealed in this study provides robust empirical evidence for optimizing forest management and informing policy decisions that reconcile climate mitigation, biodiversity conservation, and socio-economic development. As forests continue to underpin global ecological and human systems, high-resolution, origin-specific forest age information will be indispensable for guiding sustainable development and enhancing the world's adaptive capacity in an era of accelerating environmental change.

5 Conclusion

Accurate mapping of forest ages is critical to advancing global carbon neutrality, as it underpins two core pillars of climate mitigation: carbon sink quantification and targeted forest management. Traditional approaches—reliant on labor-intensive ground inventories—and existing coarse-resolution global forest age products fail to distinguish between PF and NF, severely limiting precise regional carbon accounting and evidence-based climate governance. To address this critical gap, we developed a 30 m resolution global forest age dataset by integrating the CCDC model with Landsat time-series imagery on the GEE platform, eliminating the need for ground survey data. This dataset achieved an overall accuracy of 0.72, with class-specific accuracies of 0.73 for NF and 0.70 for PF, demonstrating robust performance across forest types. By delivering high-resolution, forest-type-specific age estimates, this product fills a key niche in global ecosystem research, providing actionable data to advance ecosystem service assessment and carbon cycle modeling. More importantly, it establishes a robust technical framework for regionally tailored forest management, enabling the refined implementation of global carbon neutrality commitments.

Author contributions

YW: Conceptualization, Methodology, Formal analysis, Investigation, Resources, Sampling, Data Curation, Writing, Visualization.

HW: Formal analysis, Investigation.

CL, XL: Resources, Sampling.

ZL, XZ, SL: Supervision, Project administration.

YZ: Formal analysis, Investigation, Supervision, Project administration.

https://doi.org/10.5194/essd-2025-674
Preprint. Discussion started: 8 January 2026

Competing interests

The authors declare that they have no conflict of interest.

Acknowledgements

Funding: This research was funded by the National Key Research and Development Program of China under grant number 2024YFD1500605.

Financial support

Funding: This research was funded by the National Key Research and Development Program of China [grant number 2024YFD1500605.

Data availability

Due to the large data volume, the dataset is distributed across two repositories under the same DOI. The main dataset is hosted on Zenodo, while the remaining files are stored on Mendeley Data **u**sing the identical DOI (https://doi.org/10.17632/yfm4sw8h25.1). Wang, Y., Wang, H., Liang, C., Li, X., Liu, Z., Zhang, X., Li, S., & Zhao, Y. (2025). The Global 30m Forest Age Map (Natural vs. Planted Forest) [Data set]. Zenodo. https://doi.org/10.17632/yfm4sw8h25.1. Users can download components of the dataset from either platform.

References

[1] Aszalós, R., Thom, D., Aakala, T., Angelstam, P., Brūmelis, G., Gálhidy, L., Gratzer, G., Hlásny, T., Katzensteiner, K., Kovács, B., Knoke, T., Larrieu, L., Motta, R., Müller, J., Ódor, P., Roženbergar, D., Paillet, Y., Pitar, D., Standovár, T., Svoboda, M., Szwagrzyk, J., Toscani, P., & Keeton, W.S. (2022). Natural disturbance regimes as a guide for sustainable forest management in Europe. *Ecol Appl, 32*, e2596

[2] Bennett, B.M. (2015). *Plantations and protected areas: A global history of forest management*. MIT Press

[3] Besnard, S., Koirala, S., Santoro, M., Weber, U., Nelson, J., Gütter, J., Herault, B., Kassi, J., N'Guessan, A., & Neigh, C. (2021). Mapping global forest age from forest inventories, biomass and climate data. *Earth System Science Data Discussions, 2021*, 1-22

[4] Besnard, S., Santoro, M., Herold, M., Cartus, O., Gütter, J., Heinrich, V.H., Herault, B., Kassi, J., Koirala, S., N'Guessan, A., Neigh, C., Nelson, J.A., Poulter, B., Weber, U., Zhang, T., & Carvalhais, N. (2024). Global Age Mapping Integration (GAMI). In

[5] Bright, B.C., Hudak, A.T., Kennedy, R.E., Braaten, J.D., & Henareh Khalyani, A. (2019). Examining post-fire vegetation recovery with Landsat time series analysis in three western North American forest types. *Fire Ecology, 15*, 1-14

[6] Bunce, C. (2009). Correlation, agreement, and Bland–Altman analysis: statistical analysis of method comparison studies. *American journal of ophthalmology, 148*, 4-6

[7] Cao, Y., Zhong, D., Shang, R., Ke, Q., Zhang, M., Xie, D., Liu, S., Zhao, C., & Wei, R. (2025). Afforestation as a mitigation strategy: countering climate-induced risk of forest carbon sink in China. *Carbon Balance and Management, 20*, 18

https://doi.org/10.5194/essd-2025-674
Preprint. Discussion started: 8 January 2026

[8] Champion, I., Germain, C., Da Costa, J.P., Alborini, A., & Dubois-Fernandez, P. (2013). Retrieval of forest stand age from SAR image texture for varying distance and orientation values of the gray level co-occurrence matrix. *IEEE Geoscience and Remote Sensing Letters, 11*, 5-9
[9] Chen, W., Chen, J., Liu, J., & Cihlar, J. (2000). Approaches for reducing uncertainties in regional forest carbon balance. *Global Biogeochemical Cycles, 14*, 827-838
[10] Cheng, K., Yang, H., Tao, S., Su, Y., Guan, H., Ren, Y., Hu, T., Li, W., Xu, G., Chen, M., Lu, X., Yang, Z., Tang, Y., Ma, K., Fang, J., & Guo, Q. (2024). Carbon storage through China's planted forest expansion. *Nat Commun, 15*, 4106
[11] Du, Z., Yu, L., Yang, J., Xu, Y., Chen, B., Peng, S., Zhang, T., Fu, H., Harris, N., & Gong, P. (2022). A global map of planting years of plantations. *Scientific data, 9*, 141
[12] Erdozain, M., Alberdi, I., Aszalós, R., Bollmann, K., Detsis, V., Diaci, J., Đodan, M., Efthimiou, G., Gálhidy, L., Haase, M., Hoffmann, J., Jaymond, D., Johann, E., Jørgensen, H., Krumm, F., Kuuluvainen, T., Lachat, T., Lapin, K., Lindner, M., Madsen, P., Nichiforel, L., Pach, M., Paillet, Y., Palaghianu, C., Palau, J., Pemán, J., Perić, S., Raum, S., Schueler, S., Skrzyszewski, J., Svensson, J., Teeuwen, S., Vacchiano, G., Vandekerkhove, K., Cañellas, I., Menéndez-Miguélez, M., Werden, L.L.K., Àvila, A., & de-Miguel, S. (2024). The Evolution of Forest Restoration in Europe: A Synthesis for a Step Forward Based on National Expert Knowledge. *Current Forestry Reports, 11*, 4
[13] Escuin, S., Navarro, R., & Fernández, P. (2008). Fire severity assessment by using NBR (Normalized Burn Ratio) and NDVI (Normalized Difference Vegetation Index) derived from LANDSAT TM/ETM images. *International Journal of Remote Sensing, 29*, 1053-1073
[14] FAO (2024). The State of the World's Forests. In
[15] He, G., Zhang, Z., Zhu, Q., Wang, W., Peng, W., & Cai, Y. (2022). Estimating Carbon Sequestration Potential of Forest and Its Influencing Factors at Fine Spatial-Scales: A Case Study of Lushan City in Southern China. *International Journal of Environmental Research and Public Health, 19*, 9184
[16] Huang, Z., Li, X., Du, H., Zou, W., Zhou, G., Mao, F., Fan, W., Xu, Y., Ni, C., & Zhang, B. (2023). An algorithm of forest age estimation based on the forest disturbance and recovery detection. *IEEE Transactions on Geoscience and Remote Sensing, 61*, 1-18
[17] Ju, J., Roy, D.P., Vermote, E., Masek, J., & Kovalskyy, V. (2012). Continental-scale validation of MODIS-based and LEDAPS Landsat ETM+ atmospheric correction methods. *Remote Sensing of Environment, 122*, 175-184
[18] Köhl, M., Neupane, P.R., & Lotfiomran, N. (2017). The impact of tree age on biomass growth and carbon accumulation capacity: A retrospective analysis using tree ring data of three tropical tree species grown in natural forests of Suriname. *PLoS One, 12*, e0181187
[19] Leng, Y., Li, W., Ciais, P., Sun, M., Zhu, L., Yue, C., Chang, J., Yao, Y., Zhang, Y., Zhou, J., Li, Z., Wang, X., Xi, Y., & Peng, S. (2024). Forest aging limits future carbon sink in China. *One Earth, 7*, 822-834
[20] Li, P., Li, H., Si, B., Zhou, T., Zhang, C., & Li, M. (2024). Mapping planted forest age using LandTrendr algorithm and Landsat 5–8 on the Loess Plateau, China. *Agricultural and Forest Meteorology, 344*, 109795
[21] Liang, B., Wang, J., Zhang, Z., Zhang, J., Zhang, J., Cressey, E.L., & Wang, Z. (2022). Planted forest is catching up with natural forest in China in terms of carbon density and carbon storage. *Fundamental Research, 2*, 688-696
[22] Liao, W., Ye, D., Yuan, R., Zhang, Y., & Deng, Q. (2023). Financial compensation for natural forest logging ban: Standard calculation based on willingness to accept. *Sci Prog, 106*, 368504221145563
[23] Lu, J., Huang, C., Schleeweis, K., Zou, Z., & Gong, W. (2025). Tree age estimation across the US using forest inventory and analysis database. *Forest Ecology and Management, 584*, 122603
[24] Maza, M., Lara, J.L., & Losada, I.J. (2021). Predicting the evolution of coastal protection service with mangrove forest age. *Coastal Engineering, 168*, 103922
[25] Mo, L., Crowther, T.W., Maynard, D.S., van den Hoogen, J., Ma, H., Bialic-Murphy, L., Liang, J., de-Miguel, S., Nabuurs, G.-J., Reich, P.B., Phillips, O.L., Abegg, M., Adou Yao, Y.C., Alberti, G., Almeyda Zambrano, A.M., Alvarado, B.V., Alvarez-Dávila, E., Alvarez-Loayza, P., Alves, L.F., Amaral, I., Ammer, C., Antón-Fernández, C., Araujo-Murakami, A., Arroyo, L., Avitabile, V., Aymard, G.A., Baker, T.R., Bałazy, R., Banki, O., Barroso, J.G., Bastian, M.L., Bastin, J.-F., Birigazzi, L., Birnbaum, P., Bitariho, R., Boeckx, P., Bongers, F., Boonman, C.C.F., Bouriaud, O., Brancalion, P.H.S., Brandl, S., Brearley, F.Q., Brienen, R., Broadbent, E.N., Bruelheide, H., Bussotti, F., Gatti, R.C., César, R.G., Cesljar, G., Chazdon, R., Chen, H.Y.H., Chisholm, C., Cho, H., Cienciala, E., Clark, C., Clark, D., Colletta, G.D., Coomes, D.A., Valverde, F.C., Corral-Rivas, J.J., Crim, P.M., Cumming, J.R., Dayanandan, S., de Gasper, A.L., Decuyper, M., Derroire, G., DeVries, B.,

https://doi.org/10.5194/essd-2025-674
Preprint. Discussion started: 8 January 2026

Djordjevic, I., Dolezal, J., Dourdain, A., Engone Obiang, N.L., Enquist, B.J., Eyre, T.J., Fandohan, A.B., Fayle, T.M., Feldpausch, T.R., Ferreira, L.V., Finér, L., Fischer, M., Fletcher, C., Frizzera, L., Gamarra, J.G.P., Gianelle, D., Glick, H.B., Harris, D.J., Hector, A., Hemp, A., Hengeveld, G., Hérault, B., Herbohn, J.L., Herold, M., Hietz, P., Hillers, A., Honorio Coronado, E.N., Hui, C., Ibanez, T., Imai, N., Jagodziński, A.M., Jaroszewicz, B., Johannsen, V.K., Joly, C.A., Jucker, T., Jung, I., Karminov, V., Kartawinata, K., Kearsley, E., Kenfack, D., Kennard, D.K., Kepfer-Rojas, S., Keppel, G., Khan, M.L., Killeen, T.J., Kim, H.S., Kitayama, K., Köhl, M., Korjus, H., Kraxner, F., Kucher, D., Laarmann, D., Lang, M., Lewis, S.L., Li, Y., Lopez-Gonzalez, G., Lu, H., Lukina, N.V., Maitner, B.S., Malhi, Y., Marcon, E., Marimon, B.S., Marimon-Junior, B.H., Marshall, A.R., Martin, E.H., McCarthy, J.K., Meave, J.A., Melo-Cruz, O., Mendoza, C., Mendoza-Polo, I., Miscicki, S., Merow, C., Mendoza, A.M., Moreno, V.S., Mukul, S.A., Mundhenk, P., Nava-Miranda, M.G., Neill, D., Neldner, V.J., Nevenic, R.V., Ngugi, M.R., Niklaus, P.A., Ontikov, P., Ortiz-Malavasi, E., Pan, Y., Paquette, A., Parada-Gutierrez, A., Parfenova, E.I., Park, M., Parren, M., Parthasarathy, N., Peri, P.L., Pfautsch, S., Picard, N., Piedade, M.T.F., Piotto, D., Pitman, N.C.A., Poorter, L., Poulsen, A.D., Poulsen, J.R., Pretzsch, H., Arevalo, F.R., Restrepo-Correa, Z., Richardson, S.J., Rodeghiero, M., Rolim, S.G., Roopsind, A., Rovero, F., Rutishauser, E., Saikia, P., Salas-Eljatib, C., Saner, P., Schall, P., Schelhaas, M.-J., Schepaschenko, D., Scherer-Lorenzen, M., Schmid, B., Schöngart, J., Searle, E.B., Seben, V., Serra-Diaz, J.M., Sheil, D., Shvidenko, A.Z., Da Silva, A.C., Silva-Espejo, J.E., Silveira, M., Singh, J., Sist, P., Slik, F., Sonké, B., Sosinski, E.E., Souza, A.F., Stereńczak, K.J., Svenning, J.-C., Svoboda, M., Swanepoel, B., Targhetta, N., Tchebakova, N., ter Steege, H., Thomas, R., Tikhonova, E., Umunay, P.M., Usoltsev, V.A., Valencia, R., Valladares, F., Van Bodegom, P.M., van der Plas, F., Van Do, T., van Nuland, M.E., Vasquez, R.M., Verbeeck, H., Viana, H., Vibrans, A.C., Vieira, S., von Gadow, K., Wang, H.-F., Watson, J.V., Werner, G.D.A., Wittmann, F., Woell, H., Wortel, V., Zagt, R., Zawiła-Niedźwiecki, T., Zhang, C., Zhao, X., Zhou, M., Zhu, Z.-X., Zo-Bi, I.C., & Zohner, C.M. (2024). The global distribution and drivers of wood density and their impact on forest carbon stocks. *Nature Ecology & Evolution, 8*, 2195-2212

[26] Murphy, B.A., Rollinson, C.R., Dietze, M.C., Staudhammer, C.L., VonHedemann, N.R., Schultz, C.A., Kleindl, W.J., & Desai, A.R. (2025). Insights into nature-based climate solutions: Managing forests for climate resilience and carbon stability. *Journal of Geophysical Research: Biogeosciences, 130*, e2024JG008391

[27] Noss, R.F. (1999). Assessing and monitoring forest biodiversity: a suggested framework and indicators. *Forest Ecology and Management, 115*, 135-146

[28] Oldekop, J.A., Rasmussen, L.V., Agrawal, A., Bebbington, A.J., Meyfroidt, P., Bengston, D.N., Blackman, A., Brooks, S., Davidson-Hunt, I., Davies, P., Dinsi, S.C., Fontana, L.B., Gumucio, T., Kumar, C., Kumar, K., Moran, D., Mwampamba, T.H., Nasi, R., Nilsson, M., Pinedo-Vasquez, M.A., Rhemtulla, J.M., Sutherland, W.J., Watkins, C., & Wilson, S.J. (2020). Forest-linked livelihoods in a globalized world. *Nature Plants, 6*, 1400-1407

[29] Poulter, B., Aragao, L., Adela, N., Bellassen, V., Ciais, P., Kato, T., Lin, X., Nachin, B., Luyssaert, S., Pederson, N., Peylin, P., Piao, S., Saatchi, S., Schepaschenko, D., Schelhaas, M., & Shivdenko, A. (2018). The global forest age dataset (GFADv1.0)

[30] Racine, E.B., Coops, N.C., St-Onge, B., & Bégin, J. (2014). Estimating forest stand age from LiDAR-derived predictors and nearest neighbor imputation. *Forest Science, 60*, 128-136

[31] Reyes-Palomeque, G., Dupuy, J., Portillo-Quintero, C., Andrade, J., Tun-Dzul, F., & Hernández-Stefanoni, J. (2021). Mapping forest age and characterizing vegetation structure and species composition in tropical dry forests. *Ecological Indicators, 120*, 106955

[32] Ryu, J.-H., Han, K.-S., Hong, S., Park, N.-W., Lee, Y.-W., & Cho, J. (2018). Satellite-based evaluation of the post-fire recovery process from the worst forest fire case in South Korea. *Remote Sensing, 10*, 918

[33] Shi, X., Wang, T., Lu, S., Chen, K., He, D., & Xu, Z. (2022). Evaluation of China's forest carbon sink service value. *Environmental Science and Pollution Research, 29*, 44668-44677

[34] Smolina, A., Illarionova, S., Shadrin, D., Kedrov, A., & Burnaev, E. (2023). Forest age estimation in northern Arkhangelsk region based on machine learning pipeline on Sentinel-2 and auxiliary data. *Scientific Reports, 13*, 22167

[35] Steel, E.A., Hinckley, T.M., Richards, W.H., & D'Amore, D.V. (2024). Chapter 3 - Forests then and now: managing for ecosystem benefits, services to humans, and healthy forests across scales. In S.G. McNulty (Ed.), *Future Forests* (pp. 49-64): Elsevier

[36] Strandgard, M., & Båland, M. (2021). Economics of forest biomass for bioenergy: Potential site preparation savings from coarse woody harvesting residue removal in a short-rotation Eucalyptus globulus (Labill.) plantation. *Silva Balcanica, 22*, 45-55

https://doi.org/10.5194/essd-2025-674
Preprint. Discussion started: 8 January 2026

[37] Su, Y., Zhang, C., Ciais, P., Zeng, Z., Cescatti, A., Shang, J., Chen, J.M., Liu, J., Wang, Y.-P., & Yuan, W. (2023). Asymmetric influence of forest cover gain and loss on land surface temperature. *Nature Climate Change, 13*, 823-831
[38] Systems, U.S.D.o.S.s.O.o.t.G.a.G.P. (2017). LSIB 2017: Large Scale International Boundary Polygons, Simplified. In
[39] Tang, S., Tian, Q., Xu, K., Xu, N., & Yue, J. (2020). Age information retrieval of Larix gmelinii forest using Sentinel-2 data. *Natl. Remote Sens. Bull, 24*, 1511-1524
[40] Terrell, G.R., & Scott, D.W. (1992). Variable kernel density estimation. *The Annals of Statistics*, 1236-1265
[41] Thompson, I., Mackey, B., McNulty, S., & Mosseler, A. (2009). Forest resilience, biodiversity, and climate change. In, *Secretariat of the Convention on Biological Diversity, Montreal. Technical Series no. 43. 1-67.* (pp. 1-67)
[42] Tian, H., Zhu, J., Lei, X., Jian, Z., Chen, X., Zeng, L., Huang, G., Liu, C., & Xiao, W. (2024). Models considering the theoretical stand age will underestimate the future forest carbon sequestration potential. *Forest Ecology and Management, 562*, 121982
[43] Trisasongko, B., Panuju, D., & Iman, L. (2020). Estimating tree age of rubber stands using spaceborne L-band synthetic aperture radar. In, *IOP Conference Series: Earth and Environmental Science* (p. 012079): IOP Publishing
[44] Vermote, E., Roger, J.-C., Franch, B., & Skakun, S. (2018). LaSRC (Land Surface Reflectance Code): Overview, application and validation using MODIS, VIIRS, LANDSAT and Sentinel 2 data's. In, *IGARSS 2018-2018 IEEE International Geoscience and Remote Sensing Symposium* (pp. 8173-8176): IEEE
[45] Xiao, Y., Wang, Q., Tong, X., & Atkinson, P.M. (2023). Thirty-meter map of young forest age in China. *Earth Syst. Sci. Data, 15*, 3365-3386
[46] Xiao, Y., Wang, Q., & Zhang, H.K. (2024). Global Natural and Planted Forests Mapping at Fine Spatial Resolution of 30 m. *Journal of Remote Sensing, 4*, 0204
[47] Yu, Z., Liu, S., Li, H., Liang, J., Liu, W., Piao, S., Tian, H., Zhou, G., Lu, C., & You, W. (2024). Maximizing carbon sequestration potential in Chinese forests through optimal management. *Nature communications, 15*, 3154
[48] Zhang, J., Zhang, P., Wang, R., Liu, Y., & Lu, S. (2023). Identifying the coupling coordination relationship between urbanization and forest ecological security and its impact mechanism: Case study of the Yangtze River Economic Belt, China. *Journal of Environmental Management, 342*, 118327
[49] Zhu, Z., & Woodcock, C.E. (2014). Continuous change detection and classification of land cover using all available Landsat data. *Remote Sensing of Environment, 144*, 152-171
[50] Zou, H., & Song, Y. (2023). Influence of forest vegetation restoration on carbon increment after mining. *Scientific Reports, 13*, 19565